PRIP-TR-114

Automatic Registration of Cutaneous Hemangiomas in Digital Image Series

Sebastian Zambanini

Pattern
Recognition &
Image
Processing
Group

Institute of
Computer Aided Automation

Technical Report

Pattern Recognition and Image Processing Group
Institute of Computer Aided Automation
Vienna University of Technology
Favoritenstr. 9/1832
A-1040 Vienna AUSTRIA
Phone: +43 (1) 58801-18351
Fax: +43 (1) 58801-18392
E-mail: zamba@prip.tuwien.ac.at
URL: http://www.prip.tuwien.ac.at/

PRIP-TR-114 June 19, 2007

Automatic Registration of Cutaneous Hemangiomas in Digital Image Series

Sebastian Zambanini

Abstract

This report presents an automatic method for registering follow-up hemangioma images taken during clinical trials in specific time intervals. The method finds interest points in two images on the basis of edge points and matches corresponding interest points using SIFT features. Under the assumption that hemangioma regions are planar, these correspondences are used to determine a homography between the two images by means of RANSAC. Experimental results are reported for image pairs acquired at the same time and for image pairs acquired during follow-up showing hemangiomas at different times. Registration errors on the images are acceptable for subsequent processing, however, gross changes of hemangiomas deteriorate the performance and are subject to ongoing research.

1 Introduction

Cutaneous hemangiomas are benign vascular tumors made up of newly-formed blood vessels in the skin. They are a common disease in infancy with a frequency of about 10 % [3]. Until now the natural course of hemangiomas or their response to a certain therapy was assessed only by clinical examination. Dermatologists usually make scorings where they try to estimate the degree of regression or enlargement of the lesion. An automatic system based on photos taken of a specific hemangioma in given intervals would be useful to support the physician detecting and quantifiying the changes of a hemangioma in an objective manner. A necessary prerequisite of such a system is the registration of consecutive images to compare them in a meaningful way.
Image registration is the process of geometrically aligning two images taken from different viewpoints and, in our case, also taken at different times. This report presents an automatic method for registering hemangioma images taken during clinical trials in specific time intervals.

1.1 State of the Art

Several approaches for the registration of dermatological images were proposed in the past dealing mainly with images of skin lesions representing melanoma or psoriasis. Maglogiannis [8] and Pavlopoulos [11] both propose a similar hybrid method using the log-polar transformation for estimating scaling and rotation parameters and a sign change similarity criterion in combination with a hill-climbing optimization scheme for translation estimation. Ersbøll et al. [9] work with statistical shape analysis after lesion segmentation to do a first rigid alignment under the assumption of image scale constancy. Afterwards small internal displacements are corrected by a combined registration and alignment scheme. The SHARP-algorithm presented in [2] segments the lesions in the images and uses the first and second order moments of the resulting binary images to determine the rotation and translation parameters.

1.2 Our Contribution

The methods outlined above are not capable to handle certain properties of typical hemangioma follow up images: differences of view point during image acquisition typically exceed a range that can be accounted for by 2D rotations and translation in the image plane, the change in image scale can be high, and hemangiomas change appearance during the period of follow up examinations, making a robust approach necessary. In Fig. 1 these cases are illustrated: Fig. 1(a) and Fig. 1(b) show a pair, for which reliable matching is only possible for a small part of the hemangioma due to the healing process between examinations and rotation between images is appr. 170°. Fig. 1(c) and Fig. 1(d) are examples for a large scale change, and Fig. 1(e) and Fig. 1(f) show a pair of images where the viewpoint change is high.
Because of these issues, our approach is based on the detection and matching of distinctive interest points, by means of local features. The resulting correspondences are used for a robust estimation of the transformation between images by RANSAC. To obtain reliable

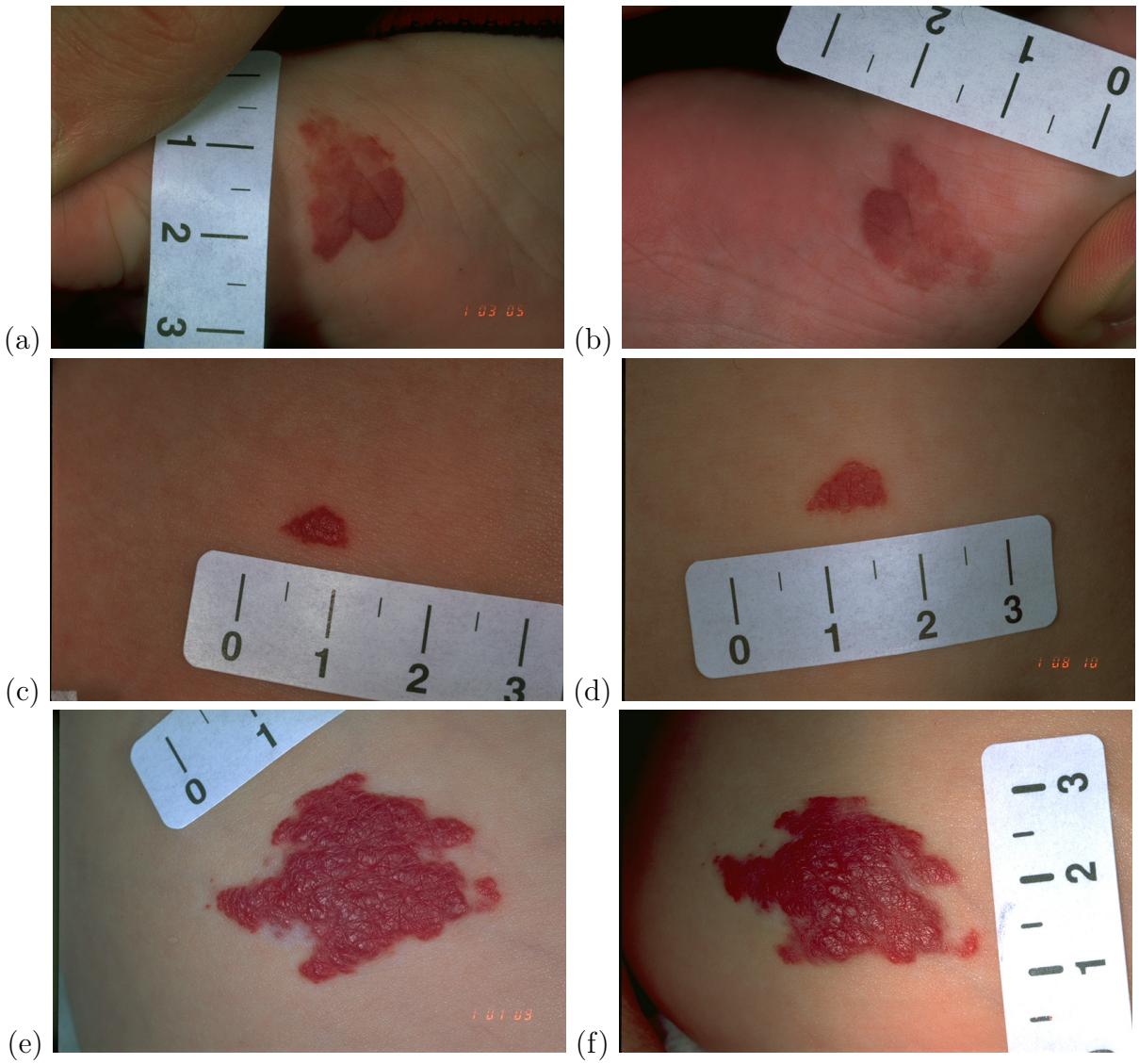

Figure 1: Three image pairs representing images of the same hemangioma taken at different times.

matches of interest points we use SIFT features [7] for description of interest points and determination of correspondences between images. Under the assumption that hemangiomas are planar, the transformation between images is defined as a homography which is estimated by the detected point correspondences.
The method has several advantages over existing approaches for dealing with hemangioma data: SIFT is a rotation and scale-invariant descriptor which allows the reliable matching of points under different views, the modeling of the transformation between images with a homography can represent any projective relation between the images, and finally RANSAC can cope with partially incorrect or missing matches between interest points caused by changed hemangioma appearances.
The feature-based image registration method can be divided into four main steps [13].

They also roughly set the structure of the report:

1. **Feature detection:** Interest points are detected in both images (Section 2).
2. **Feature matching:** Interest points are matched by means of their feature descriptions (Section 3).
3. **Transform model estimation:** Matched interest points are used to compute the parameters of the mapping function which is in our case a homography (Section 4).
4. **Image resampling and transformation:** The image is finally transformed using the computed mapping function and usually bilinearly interpolated.

In Section 5 several experiments performed on the data gathered with the algorithm proposed are presented and discussed. A conclusion is finally given in Section 6.

2 Detection and Description of Interest Points in Hemangioma Images using SIFT

As mentioned above, the first task is to find distinctive interest points in the images to be registered. In this section first the original SIFT method is described followed by the motivation and explanation of our adaptation for interest point detection.

2.1 Scale Invariant Feature Transform

The scale-invariant feature transform (SIFT) presented by Lowe [7] is a scale and rotation invariant local descriptor of features in images and has proven to be a robust and therefore widely used method [10]. It consists of four major steps:

1. **Scale-space extrema detection:** The detection of interest points works on different octaves, i.e. different resolutions of the image. For each octave a Gaussian scale space is computed by repeatedly convolving the image with a Gaussian filter kernel and subsequently Difference-of-Gaussians images are created by subtracting the blurred images with adjacent scales. Candidate locations for interest points are then detected at extrema of the Difference-of-Gaussians images.
2. **Keypoint localization:** For each initial keypoint (interest point) position a interpolated more exact position is determined by a 3D quadratic function. Furthermore, unstable extrema with low contrast are rejected.
3. **Orientation assignment:** In order to achieve rotation invariance of interest point descriptors, to each interest point a main orientation determined by means of peaks in an orientation histogram of surrounding gradient orientations is assigned. All future operations are performed relative to the main orientation.

4. **Keypoint descriptor:** Again the local gradient data is used to create a set of histograms over a window centered on the keypoint. Usually a set of 16 histograms, aligned in a 4x4 grid, each with 8 orientation bins is used. This results in a feature vector of 128 elements for each interest point.

2.2 Interest Points based on Canny Edge Detector

For our task the standard SIFT method has to be modified on some points, to account for the specific nature of the image data. The interest point detection is constrained to a region covering the hemangioma, only the green color component of the images is taken into account, and Canny edges are used for the interest point localization.

1. Constraining interest points to the hemangioma region: The analysis is constrained to a region of interest, including the hemangioma. Segmentation of the hemangioma region is done by a pixel-wise classification method proposed in an earlier work [12]. Once the image has been segmented, only interest points inside or near the hemangioma region are accepted. This ensures that the planarity assumption for the homography estimation gives a good estimate of the actual surface, accounts for a better chance of reliable matches in the close vicinity of the hemangioma and reduces computational costs.
In detail, interest points are only accepted if:

1. they are located in the frame encompassing the segmented hemangioma region, enlarged by 40 pixels on each side.

2. they are not located in a background region, i.e. not located in a region that has been detected as non skin by the heuristic described in [12]. Note that thereby also the ruler is excluded and differences in its placement do not affect the registration.

2. Local image representation: The standard SIFT method works on gray-value images, but in our case the green channel of the RGB-images is a more reasonable choice. As mentioned in [12], this representation shows higher differences between hemangioma regions and healthy skin which can also be seen in Fig. 2 where the gray-value representation and the green channel representation of a hemangioma image is shown. Therefore, the whole registration process works on normalized green channel images.

3. Interest point localization: In the original SIFT method interest points (called *keypoints*) are localized at extrema in the Difference-of-Gaussians scale space. However, this interest point localization procedure generates an unsatisfactory number of distinctive interest points and correct matches on our images. The reason is that Difference-of-Gaussians tends to have more extrema at intensity variations inside the hemangioma than at the exact hemangioma border. However, the most reliable interest points lie at the hemangioma border because the inner hemangioma parts change to a higher degree from one time to another. Therefore, in our method interest points are detected along edges in the images. Edge detection is accomplished by means of the Canny edge detector [1] and interest points are finally localized at edge pixels showing the highest gradient magnitude

(a)  (b) 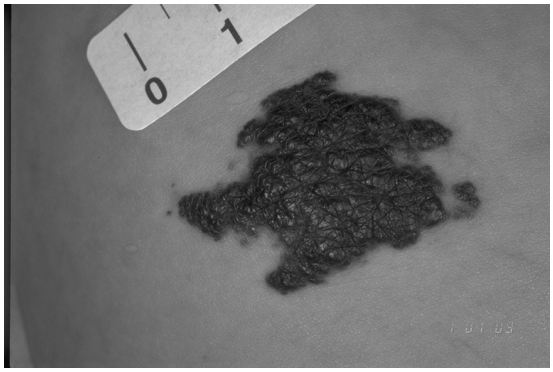

Figure 2: (a) Gray-value representation and (b) green channel representation of a RGB hemangioma image.

in a neighborhood of N pixels. By empirical tests a value of $N = 3$ combined with a low threshold of 0.1 and a high threshold of 0.2 for the Canny edge detection method has proven to be adequate for obtaining a high number of distinctive interest points. The improvement achieved by this method is evaluated in Section 5.1. In this experiment more matches are rated as correct by using the method described above (∼41 %) than by using the usual Difference-of-Gaussians approach (∼16 %).
In Fig. 3 the results of the individual steps of our interest point localization procedure are shown for the image of Fig. 1(e). Fig. 3(a) shows the segmentation of the hemangioma area (green border) and resulting rectangular region of interest (blue frame). For interest point localization only the green channel of this frame is used which is shown in Fig. 3(b). Non skin regions like the ruler in the upper left corner are ignored. Next, the Canny edge detector is applied resulting in the edge image shown in Fig. 3(c). Finally, interest points are detected at edge pixels having the highest gradient magnitude in a neighborhood of 3 pixels, marked as black spots in Fig. 3(d). Thus, a total number of 1441 interest points are detected in the image.

3 Matching of Interest Points in Two Hemangioma Images

Once the interest points have been localized, they have to be matched in a robust way. Like in the standard SIFT method, our interest points are described by accumulating the orientations in a region around the interest point location. We are using a 4x4 descriptor array with 8 orientation bins in each, resulting in a 128-element feature vector for each interest point.
The task of the matching step is to find for every interest point of the first image (the *sensed* image) the corresponding interest point of the second image (the *reference* image). A simple way to determine the correspondences is to match interest points whose descriptor vectors have the lowest Euclidean distance to each other. However, many interest points of the sensed image might not have any corresponding interest point in the

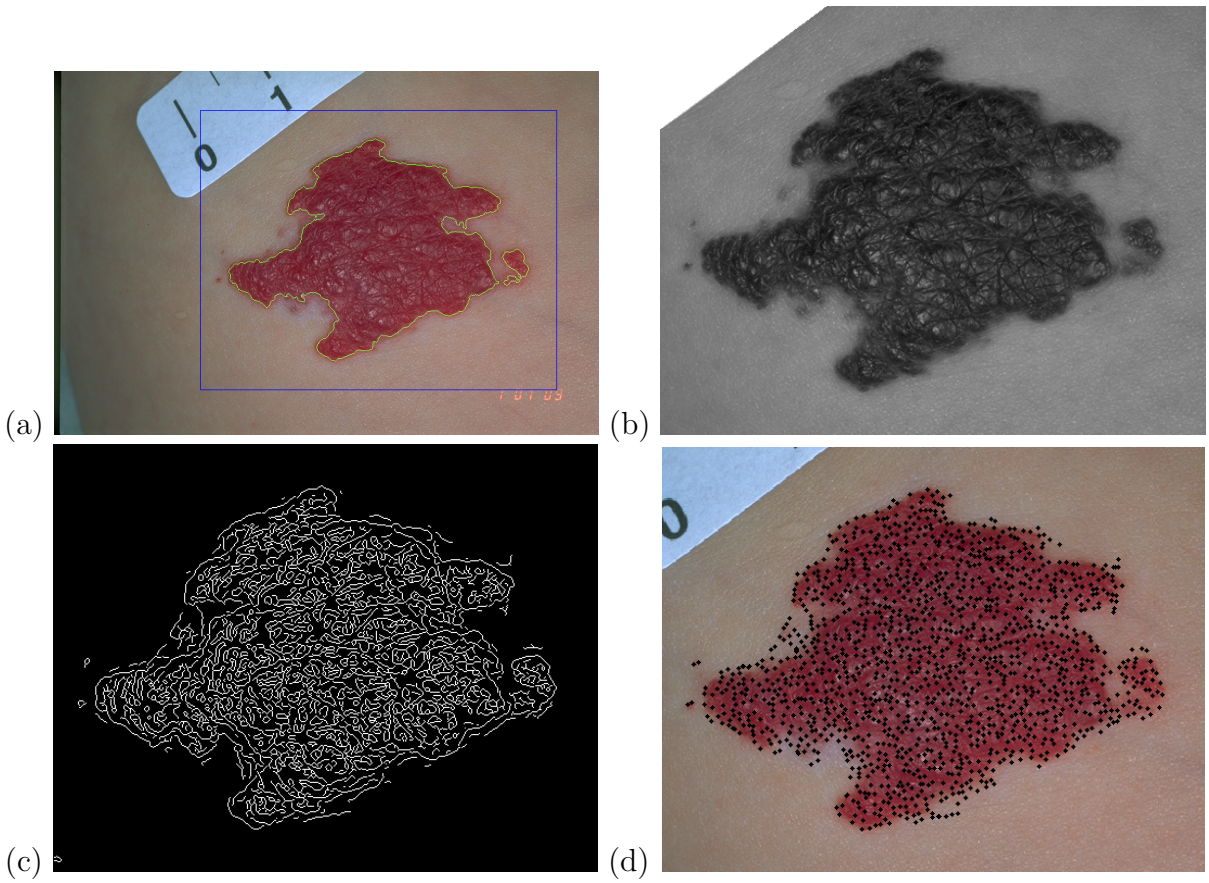

Figure 3: Individual steps of the interest point localization procedure.

reference image and vice versa. As described by Lowe in [7], a convenient measure for the quality of a match is not only the distance to the nearest neighbor in the reference image but also the distance to the second nearest neighbor. A "good" match for an interest point in the sensed image shows a low distance to its first nearest neighbor and a comparatively high distance to its second nearest neighbor in the reference image.
With our method the interest points are matched in a similar way. Although RANSAC is capable of handling a large portion of incorrect matches, a preselection of the matches with highest confidence can improve the stability. Therefore, matches are determined by means of lowest Euclidean distance of interest point descriptors, sorted in terms of the distance between the nearest and the second nearest neighbor, and finally only the "best" n matches are accepted. The number n of accepted matches should thereby be chosen dependent on the size of the hemangioma in the sensed image: in an image pair containing a large hemangioma more matches could be reliably detected than in an image pair containing a small hemangioma. Therefore, the value n is determined by $n = 2\sqrt{m_{si}}$, rounded to the nearest integer value, where m_{si} is the number of interest points detected in the sensed image. This function has been decided for by empirical tests achieving the best performance on the given data. It gives enough matches for small hemangiomas (small m_{si}) but avoids too many unreliable matches for large hemangiomas (large m_{si}) as

well. In the provided images m_{si} can vary from about 50 up to about 1500, corresponding to a n-value of 14 to 77. The function is shown in Fig. 4 for an interest point number range of 1 to 2000.

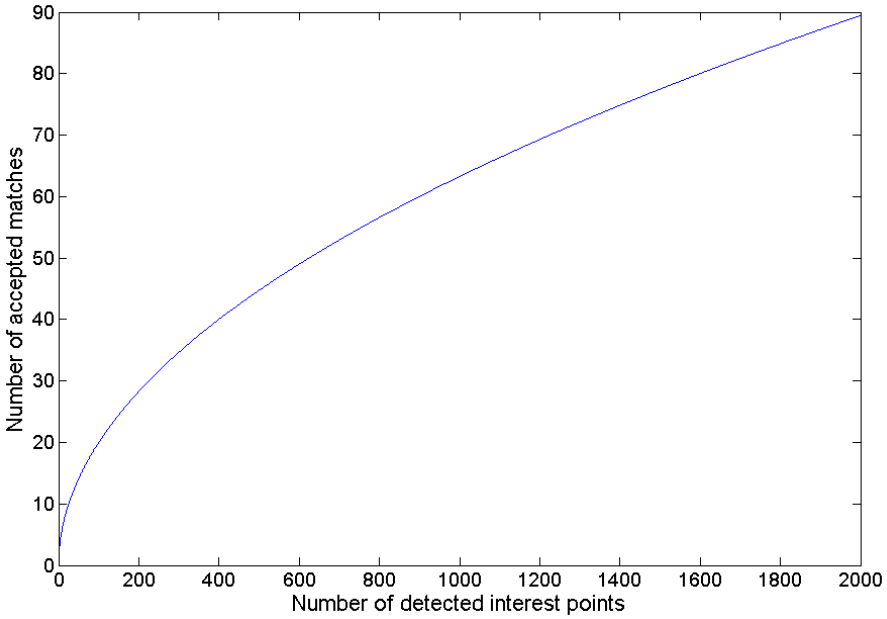

Figure 4: Function for determining the number n of accepted matches.

Fig. 5 shows exemplarily the matching result between the image from Fig. 3 and the corresponding image from the following examination. In this case 76 matches are initially accepted. However, it can be seen that still many of these matches are incorrect. The overcoming of this problem is described in the next section.

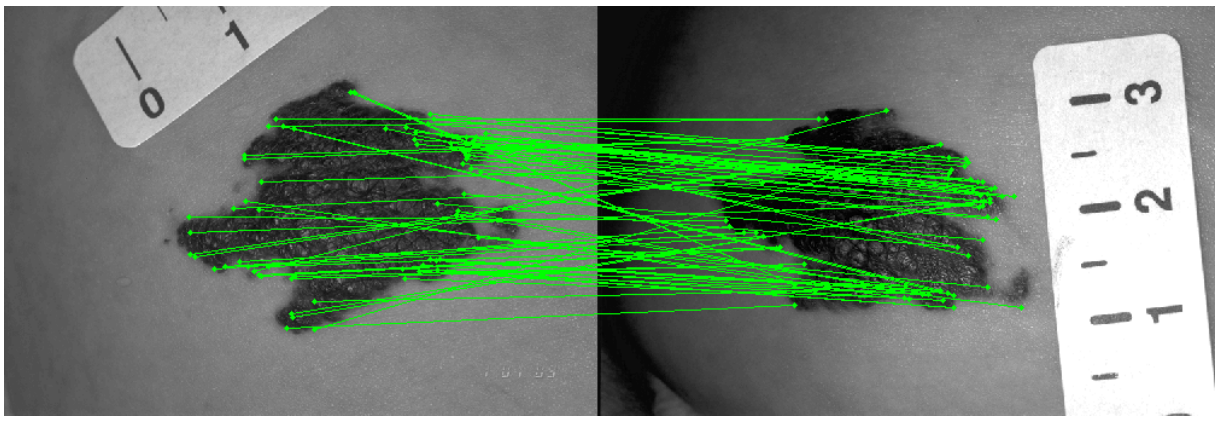

Figure 5: Determined corresponding interest points between two consecutive images.

4 Robust Homography Estimation Based on Interest Point Matches

The final step in the image registration procedure is the computation of the homography that maps the sensed image onto the reference image. In general, with a homography the transformation of all points lying on a plane in the scene shown in the sensed image to the same points in the reference image can be described. This means that the hemangiomas are assumed to be planar, which is not correct in all cases, but a reasonable simplification. An evaluation of the error made by this assumption and the possible use of more flexible transformation models is subject of ongoing research.
This section describes the method for the robust estimation of the homography between the hemangiomas contained in the sensed and reference image. In Section 4.1 the general mathematical method for homography estimation is explained. A reliable remedy for the problem of incorrect matches (*outliers*) is given in Section 4.2.

4.1 Homography Estimation from a Set of Point Matches

A homography has eight degrees of freedom and is represented by a non-singular homogeneous 3x3 matrix. Thus, it can be exactly defined by a set of four corresponding points with at most two of them being collinear. For a set of more than four matches, the homography can be estimated by the normalized Direct Linear Transform (DLT) which minimizes the algebraic error [6].
Given n matches of points $\{\mathbf{p}_i^{si} \leftrightarrow \mathbf{p}_i^{ri}\}$ between the sensed image (si) and the reference image (ri), a homography H is estimated by the normalized DLT in the following way:

1. Normalization of $\mathbf{p}_i^{si}$: Compute a similarity transformation T transforming the points $\mathbf{p}_i^{si} = (x_i^{si}, y_i^{si}, 1)^T$ to a new set of points $\tilde{\mathbf{p}}_i^{si}$ such that the centroid of the points $\tilde{\mathbf{p}}_i^{si}$ is at $(0, 0, 1)^T$ and their average distance is $\sqrt{2}$. The similarity transform T has the form

$$T = \begin{pmatrix} \sqrt{2}/\hat{d} & 0 & -\sqrt{2}\hat{x}/\hat{d} \\ 0 & \sqrt{2}/\hat{d} & -\sqrt{2}\hat{y}/\hat{d} \\ 0 & 0 & 1 \end{pmatrix}$$

with

$$\hat{x} = \frac{1}{n}\sum_{i=1}^{n} x_i^{si},\ \hat{y} = \frac{1}{n}\sum_{i=1}^{n} y_i^{si},\ \hat{d} = \frac{1}{n}\sum_{i=1}^{n} \sqrt{(x_i^{si} - \hat{x})^2 + (y_i^{si} - \hat{y})^2}$$

2. Normalization of $\mathbf{p}_i^{ri}$: Likewise, compute a similarity transformation T' transforming $\mathbf{p}_i^{ri}$ to $\tilde{\mathbf{p}}_i^{ri}$.

3. Direct Linear Transformation: For each match $\{\tilde{\mathbf{p}}_i^{si} \leftrightarrow \tilde{\mathbf{p}}_i^{ri}\}$ the homography $\tilde{H}$ is given by $\tilde{\mathbf{p}}_i^{ri} = \tilde{H}\tilde{\mathbf{p}}_i^{si}$. This can be written in the form

$$A_i\mathbf{h} = \begin{pmatrix} \mathbf{0}^{\mathrm{T}} & -\tilde{\mathbf{p}}_i^{si^{\mathrm{T}}} & y_i^{ri}\tilde{\mathbf{p}}_i^{si^{\mathrm{T}}} \\ -\tilde{\mathbf{p}}_i^{si^{\mathrm{T}}} & \mathbf{0}^{\mathrm{T}} & -\tilde{x}_i^{ri}\tilde{\mathbf{p}}_i^{si^{\mathrm{T}}} \\ -\tilde{y}_i^{ri}\tilde{\mathbf{p}}_i^{si^{\mathrm{T}}} & \tilde{x}_i^{ri}\tilde{\mathbf{p}}_i^{si^{\mathrm{T}}} & \mathbf{0}^{\mathrm{T}} \end{pmatrix} \begin{pmatrix} \mathbf{h}^1 \\ \mathbf{h}^2 \\ \mathbf{h}^3 \end{pmatrix} = \mathbf{0}$$

A_i is a 3x9 matrix and $\mathbf{h}$ is a 9-element vector made up of the entries of the matrix $\tilde{H}$,

$$\mathbf{h} = \begin{pmatrix} \mathbf{h}^1 \\ \mathbf{h}^2 \\ \mathbf{h}^3 \end{pmatrix}, \ \tilde{H} = \begin{pmatrix} h_1 & h_2 & h_3 \\ h_4 & h_5 & h_6 \\ h_7 & h_8 & h_9 \end{pmatrix}$$

with h_i the i-th element of $\mathbf{h}$. Since only two rows of A_i are linearly independent, each match gives two equations in the entries of $\tilde{H}$. We therefore use only the first two rows of A_i and assemble the n 2x9 matrices into a single $(2n)$x9 matrix A. The solution $\mathbf{h}$ is the unit singular vector corresponding to the smallest singular value of A obtained by a Singular Value Decomposition.

4. Denormalization: Denormalize $\tilde{H}$ with $H = T'^{-1}\tilde{H}T$.

To transform an image point $\mathbf{p}_i^{si}$ of the sensed image it has to be represented by homogeneous coordinates $\mathbf{p}_i^{si} = (x_i^{si}, y_i^{si}, 1)^T$. The transformation is achieved by $\mathbf{p}_i^{ri} = H\mathbf{p}_i^{si}$ and division of the resulting point $\mathbf{p}_i^{ri}$ by its homogeneous component.

4.2 Robust Detection of Outliers

As mentioned above, the matching of interest points also produces false matches that have to be detected and discarded. Since every match is equally considered for homography estimation by the DLT algorithm, it is not robust against these so called outliers, i.e. even one outlier can disturb the registration result to a high degree. Therefore, a necessary requirement of the final homography estimation method is a robust detection of inliers and outliers in the present interest point matches.
RANSAC (RANdom SAmple Consensus) is a robust model fitting method which is able to cope with a large portion of outliers [4]. Therefore, its scheme is applied on the interest point matches to obtain outlier-tolerant homography estimations. The underlying idea is to randomly and repeatedly choose four matches out of the set of putative matches, compute a homography for each set of four matches and finally take the homography H that has the largest number of inliers in the remaining set. An inlier in this case is defined as a match where the interest point in the sensed image is located within a given distance to the matching interest point in the reference image after a transformation with H.
On our images best results were achieved by iterating 2000 times and allowing a maximum distance of 5 pixels for the inlier decision (in a typical image 5 pixels correspond to ∼0.375

for *i=1* **to** *2000* **do**
▷ select a random sample of 4 matches out of all matches and compute the homography H
if *(absolute value of the determinant of H between 0.1 and 10)* **then**
▷ calculate the distance d to all other matches
▷ compute the number of inliers as the number of matches for which $d < 5$
if *(H has number of inliers larger than the present best homography)* **then**
▷ mark H as best homography
else if *(number of inliers is equal)* **then**
▷ choose the homography with the lower standard deviation of inliers
end
end
end
▷ re-estimate the best homography from all matches classified as inliers using the normalized DLT

Algorithm 1: The RANSAC-algorithm for estimating a homography from putative matches between two hemangioma images.

mm). To increase robustness only homographies with an absolute value of the determinant in the range of 0.1 to 10 are allowed. If the determinant of a homography or its inverse is close to zero, it corresponds to a degenerated case. The full algorithm is summarized in Alg. 1.
Once the final homography is computed, the last step in the registration process is to transform the sensed image onto the reference image. In practice, this is done by computing the inverse of the homography, transforming each image point of the new image onto the sensed image and computing its image value by bilinear interpolation. In Fig. 6 the final results for the images Fig. 1(e) and Fig. 1(f) are shown. Fig. 6(b) shows the remaining inliers determined by RANSAC of the initial matches depicted in Fig.6(a). In this example 31 of the 76 initial matches are classified as inliers. The final transformed sensed image can be seen in Fig. 6(c). The difference between the transformed image and the reference image is shown in Fig. 6(d).

5 Experiments

For experiments in total 63 different images taken at the *Vienna General Hospital* using an analog photo camera and digitalized with a scanner were available. All images have a resolution of 512x768 pixels and a bit depth of 8 bits per color channel.
At first, an comparative evaluation of Canny edge interest points and standard Difference-of-Gaussians interest points is given in Section 5.1. For an evaluation of the image registration method under "perfect" conditions with unchanged hemangioma appearances experiments were conducted on a set of 20 image pairs, each pair showing the same hemangioma at the same time, i.e. only a few seconds between image acquisitions. The results are shown and discussed in Section 5.2. In order to assess the amount of deterioration for registrations of consecutive images (i.e. with a period of several months between

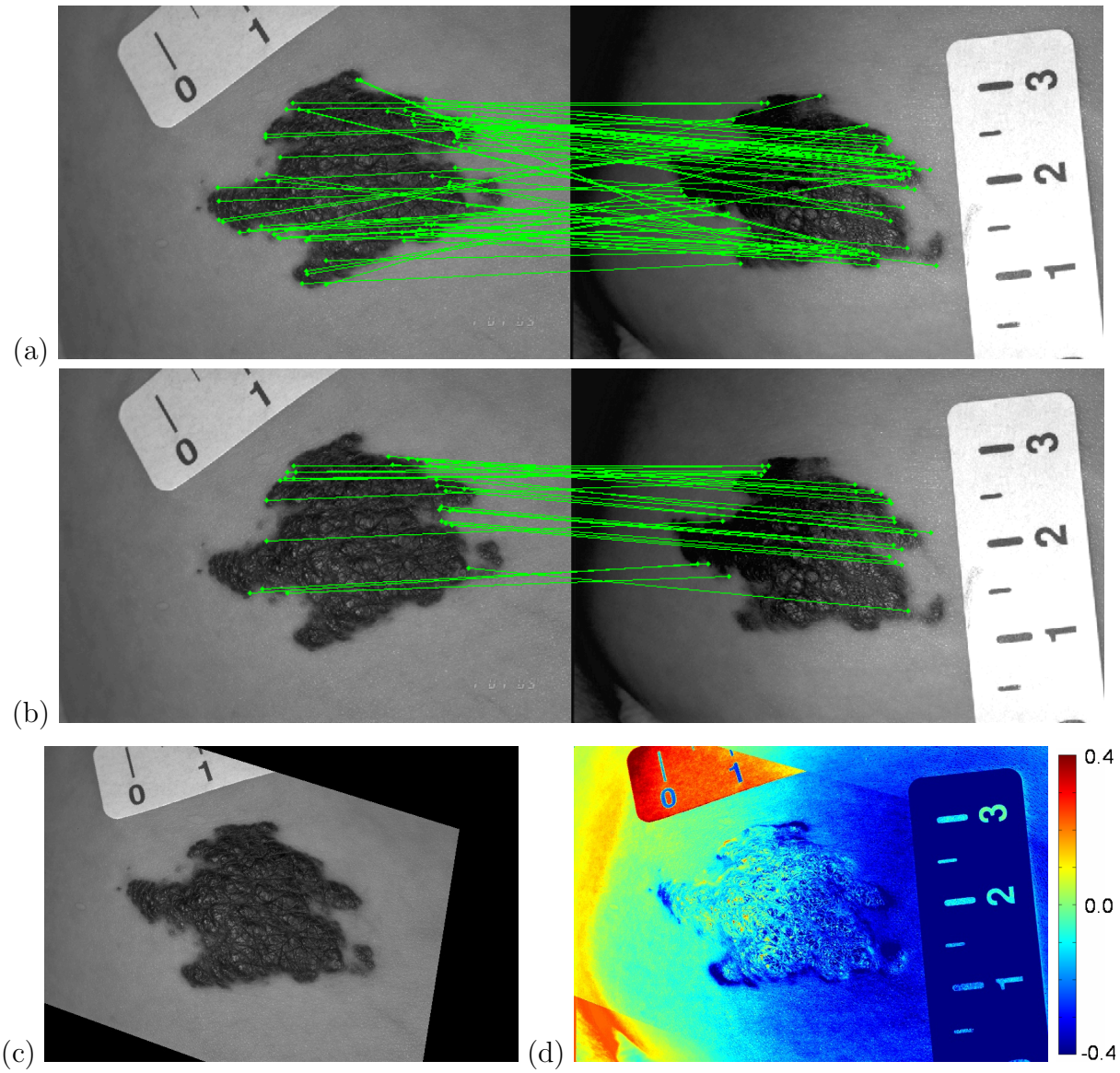

Figure 6: (a) between sensed image (left) and reference image (right), (b) detected inliers, (c) transformed sensed image and (d) image displaying the difference between the transformed sensed image and the reference image.

image acquisitions), tests on four image series are reported in Section 5.3.

5.1 Comparison of Difference-of-Gaussians Interest Points and Canny Edge Interest Points

As described in Section 2.2 interest points are detected at Canny edge points having a local maximum of gradient magnitudes. In this section the improvement achieved by this method compared to the original Difference-Of-Gaussians localization is demonstrated by a simple test where we have compared the number of correct matches of three image pairs

of consecutive hemangioma images. For every image pair the best 40 matches having the lowest euclidean distance are determined and the correct matches are counted for both methods by visual inspection. As can be seen in Table 1, with our localization method ∼41 % of the matches are rated as correct whereas with the DoG localization method (using the standard parameter values defined in [7]) only ∼16 % are rated as correct. As a conclusion, on our images Canny interest points are much more stable than Difference-of-Gaussians interest points.

Image Pair	Correct Matches DoG	Correct Matches Canny
1	7/40	16/40
2	7/40	21/40
3	5/40	12/40
Total	19/120	49/120
Percent	**∼16 %**	**∼41 %**

Table 1: Comparison of Difference-of-Gaussians interest points and Canny edge interest points by manually determined correct matches.

5.2 Precision of the Image Registration Method on Hemangioma Images taken at the same Time

In order to increase reliability two or more images of a hemangioma were taken during an examination. 20 of such image pairs are used for testing the precision of the proposed image registration method. The registration error is measured using three different metrics:

1. **Distance Error of Inliers:** The average pixel distance of transformed inliers to the real points of the matches classified as inliers.

2. **Distance Error of 5 Test Points:** For each image pair 5 matches are manually placed and the average pixel distance achieved with the estimated homography is measured.

3. **Border Error:** Both the sensed and reference image are segmented and the border error [5] between the transformed sensed segmentation and the reference segmentation is measured. Border error is computed as $\frac{Area(R_{ss} \cup R_{rs}) - Area(R_{ss} \cap R_{rs})}{Area(R_{rs})}$ where R_{ss} and R_{rs} are the segmented regions of the transformed sensed segmentation and the reference segmentation, respectively.

The results of the test are listed in Table 2. Additionally to the proposed error metrics for each image pair the number of detected interest points in the sensed and reference image, the resultant number of initial matches and the fraction of these matches classified as inliers are indicated. It can be seen that the average distance error of the 5 test points

Image Pair	Interest points sensed image	Interest points reference image	Initial Matches	Inliers	Average Distance Error of Inliers	Average Distance Error of 5 Test Points	Border Error
1	590	659	49	48	1.69 px	3.28 px	10.78 %
2	391	489	40	40	0.55 px	1.51 px	7.85 %
3	1441	1343	76	76	0.73 px	1.63 px	1.76 %
4	142	84	24	20	2.98 px	2.74 px	8.93 %
5	225	294	30	30	0.70 px	2.41 px	3.30 %
6	393	360	40	39	2.07 px	2.28 px	3.69 %
7	165	144	26	26	0.71 px	1.82 px	4.53 %
8	1009	1172	64	64	1.63 px	1.67 px	3.41 %
9	225	273	30	22	2.43 px	2.64 px	7.51 %
10	117	154	22	18	2.64 px	1.66 px	8.66 %
11	325	290	36	36	1.82 px	1.33 px	6.72 %
12	916	1109	61	61	1.61 px	3.15 px	10.02 %
13	224	208	30	30	1.27 px	3.26 px	17.05 %
14	89	66	19	18	2.00 px	2.45 px	3.29 %
15	326	313	36	35	2.11 px	2.58 px	7.96 %
16	326	157	36	35	1.44 px	2.66 px	14.09 %
17	354	339	38	33	2.31 px	2.94 px	10.82 %
18	66	117	16	16	0.61 px	2.62 px	13.71 %
19	152	227	25	22	2.05 px	1.35 px	15.68 %
20	320	351	36	36	0.81 px	2.18 px	6.15 %
Average	**389.8**	**407.5**	**36.7**	**35.3**	**1.61 px**	**2.31 px**	**8.30 %**

Table 2: Results of the proposed image registration method on 20 image pairs, each pair showing the same hemangioma at the same time.

lies at 2.31 pixels (∼0.175 mm) which is not a large increase compared to the distance error of the inliers (1.61 pixels or ∼0.125 mm). Another indication of accuracy is the fraction of the initial matches classified as inliers. On average 35.3 of the 36.7 initial matches are classified as inliers which corresponds to a percentage of ∼96 %.
In Fig. 8-11 for each registration the sensed image, the reference image and the difference image between the transformed sensed and the reference image is shown. The numbering of difference images corresponds to the numbering of the 20 image pairs in Table 2. It can be seen that the difference images show small disparities in the range of ∼0.1 inside and around the hemangioma region (note that larger local differences are caused by highlights on the hemangiomas). The only exceptions are Fig. 8(1), 9(10), 10(14) and 10(16) where larger differences up to a value of ∼0.35 arise at the hemangioma border because the assumption of hemangioma planarity is violated.

5.3 Precision of the Image Registration Method on Hemangioma Images taken at different Times

To assess the accuracy of the proposed method of consecutive images of the same hemangioma taken at different times we applied our algorithm on four different image series. Each image series consists of four or five images, resulting in a total of 13 registrations marked by two characters, patient (1,2,3,4) and position in the sequence of registrations (A,B,C,D). For instance, 2C indicates the registration of the images from the third and the fourth examination of patient 2. The same error metrics as in Section 5.2, apart from border error, are measured and listed in Tab. 3. Additionally, a further error metric measuring the consistency of three circularly concatenated registrations is used, which is illustrated in Fig. 7. In this experiment two images from examination 1 (Image A and Image A') and one from the subsequent examination 2 (Image B') are used. The three homographies H_1, H_2 and H_3 between the images are computed and the composite homography $H = H_3H_2H_1$ is build. In the absence of error, H is the identity matrix and every point in Image A is not displaced by a transformation with it. Inevitably, there is an error which can be measured by the average displacement of points in Image A. Therefore, a set of reference points is equally placed in 10 pixel distances inside the hemangioma region of Image A (green points in Fig. 7) and transformed by the composite homography H. The error is computed as the average Euclidean distance between reference points and their corresponding transformed points, listed as *Average Reference Points Displacement* in Tab. 3. This error is not stated for the registrations 3C, 4B and 4C because in this cases only one image from examination 1 is available.

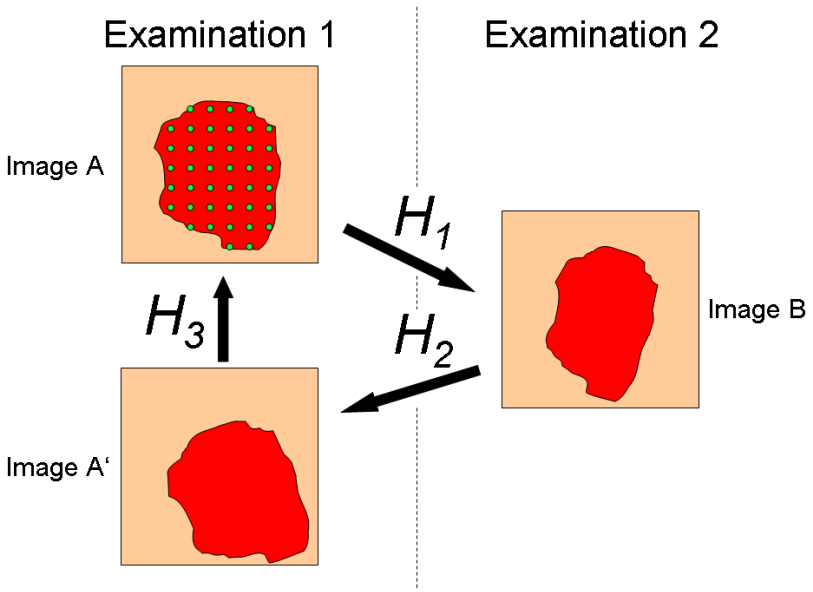

Figure 7: Illustration of the scheme for testing consistency of three circularly concatenated registrations.

Image series	Interest Points Sensed Image	Interest Points Reference Image	Initial Matches	Inliers	Average Distance Error of Inliers	Average Distance Error of 5 Test Points	Average Reference Points Displacement
1A	500	590	45	17	3.03 px	7.96 px	2.41 px
1B	590	671	49	28	2.79 px	3.96 px	8.67 px
1C	671	664	52	31	2.90 px	6.45 px	5.79 px
2A	1441	945	76	30	3.30 px	7.39 px	2.00 px
2B	945	1350	61	15	2.77 px	8.77 px	5.42 px
2C	1350	1497	73	35	2.41 px	12.94 px	5.67 px
2D	1497	187	77	7	1.41 px	354.84 px	440.38 px
3A	393	266	40	12	3.61 px	3.95 px	3.60 px
3B	266	191	33	18	2.57 px	4.92 px	3.76 px
3C	191	550	28	16	2.70 px	5.21 px	
4A	363	477	38	8	3.33 px	10.08 px	11.50 px
4B	477	213	44	11	3.97 px	4.69 px	
4C	213	767	29	6	0.94 px	196.43 px	
Average	684.38	643.69	49.62	18.00	**2.75 px**	**48.27 px**	**48.92 px**
Average (without 2D and 4C)	653.36	674.00	49.00	20.09	**3.03 px**	**6.94 px**	**5.43 px**

Table 3: Results of the proposed image registration method on 4 image series with overall 13 registrations.

Not surprisingly, the results are worse than for the image pairs tested in Section 5.2 since the content of the images changes from one time to another. Nevertheless, the average distance error of 5 test points and the average reference points displacement never exceeds 12 pixels (∼0.9 mm), with the exception of the registrations 2D and 4C. In this two cases the hemangiomas have changed too much to obtain reliable matches and a meaningful homography. By excluding these two very bad results we achieve an average reference points displacement of 5.43 pixels (∼0.4 mm). The results of the match detection deteriorate, indicated by a lower fraction of initial matches finally classified as inliers (∼41 %).
In Fig. 12-14 for each registration the sensed image, the reference image and the difference image between the transformed sensed and the reference image is shown. Naturally, compared to the difference images of image pairs showing the same hemangioma at the same time of Fig. 8-11, higher differences occur since the appearance of a hemangioma changes from one time to another. For example, in Fig. 13(1C) differences occur at the regressing regions of the reference image. In Fig. 14(2C) the lower parts of the hemangioma are not correctly registered, indicated by higher differences in this border region compared to the other border regions of the difference image. The reason for such local errors is an irregular distribution of matches (and therewith inliers) in the hemangioma region, i.e. regions not represented sufficiently by matches are neglected by the homography estimation and tend to local misregistrations.

The accuracy of the registrations is expected to be adequate for an automatic analysis of hemangioma changes over time which is part of future work. The potential to improve the registration result by local non-rigid refinements, and the involved risk of *over registration* if changes of the hemangioma are large, is subject of ongoing research.

6 Conclusion

In order to support dermatologists in the analysis of the development of cutaneous hemangiomas a correct registration of hemangioma images is an essential preprocessing step for accurate assessment methods. The main challenges of the data are high variations of hemangioma appearance, changes of illumination conditions and different viewpoints between hemangioma images. Under the assumption that particular regions of the hemangioma do not change heavily from one examination to the next, SIFT features allow for a reliable match of subsets of interest points and homographies can be estimated based on these unaltered regions. Provided that the hemangiomas are close to planar, the use of homographies as transformation model is an appropriate choice because it allows any projective relation between hemangiomas to be registered.
Experimental results show that the majority of the images can be registered without considerable errors. The average reference point displacement of 5.43 pixels represents an acceptable error if it is taken into account that this error is accumulated by three different registrations and on average the hemangiomas in the tested images have a height and width of about 200 and 180 pixels, respectively. Nevertheless, the conducted tests have also shown that registrations on image pairs containing strongly changed hemangiomas sometimes result in a failure of the registration. The visual control of registration results by a human expert is inevitable to detect such erroneous registrations. However, these infrequent cases could be manually registered by user-defined matches between the two images. Although experiments were only conducted on hemangioma images it must also be stated that the proposed method can be applied to other types of lesions as well (e.g. melanoma or psoriasis).
In future work the development of an automatic system for change detection supporting the dermatologist in the analysis of hemangioma changes in follow-up studies is planned. For this purpose, an automatic registration of hemangioma images is essential and the proposed method is expected to be accurate enough in most cases. Future work will focus on the improvement of registration results by local refinements at hemangioma borders and by the use of more flexible transformation models.

Acknowledgments

The author would like to thank Georg Langs and Prof. Robert Sablatnig for their help and support and Prof. Harald Maier from the *Division of Special and Environmental Dermatology* at the *Medical University of Vienna* for his collaboration and for providing the images.

References

[1] J. Canny. A computational approach to edge detection. *IEEE Transactions on Pattern Analysis and Machine Intelligence*, 8(6):679–698, 1986. 4

[2] D. Delgado, B. K. Ersbøll, and J. M. Carstensen. S.H.A.R.P: A smart hierarchical algorithm to register psoriasis. In *Proc. of International Workshop on Systems, Signals and Image Processing*, pages 43–46, September 2004. 1

[3] B.A. Drolet, N.B. Esterly, and I.J. Frieden. Hemangiomas in children. *New England Journal of Medicine*, 341:173–181, July 1999. 1

[4] M.A. Fischler and R.C. Bolles. Random sample consensus: A paradigm for model fitting with applications to image analysis and automated cartography. *Communications of the ACM*, 24(6):381–395, 1981. 9

[5] G.A. Hance, S.E. Umbaugh, R.H. Moss, and W.V. Stoecker. Unsupervised color image segmentation with application to skin tumor borders. *IEEE Engineering in Medicine and Biology*, 15(1):104–111, January/February 1996. 12

[6] R.I. Hartley and A. Zisserman. *Multiple View Geometry in Computer Vision*. Cambridge University Press, ISBN: 0521540518, second edition, 2004. 8

[7] D. G. Lowe. Distinctive image features from scale-invariant keypoints. *International Journal of Computer Vision*, 60(2):91–110, 2004. 2, 3, 6, 12

[8] I. Maglogiannis. Automated segmentation and registration of dermatological images. *Journal of Mathematical Modelling and Algorithms*, 2(3):277–294, 2003. 1

[9] G. Maletti, B. K. Ersbøll, and K. Conradsen. A combined alignment and registration scheme of lesions with psoriasis. *Information Sciences*, 175(3):141–159, 2005. 1

[10] K. Mikolajczyk and C. Schmid. A performance evaluation of local descriptors. In *Proc. of Conference on Computer Vison and Pattern Recognition*, pages 257–263. IEEE Computer Society, 2003. 3

[11] S.A. Pavlopoulos. New hybrid stochastic-deterministic technique for fast registration of dermatological images. *Medical & Biological Engineering & Computing*, 42(6):777–786, 2004. 1

[12] S. Zambanini, G. Langs, R. Sablatnig, P. Donath, and H. Maier. Automatic surveying of cutaneous hemangiomas. In *Proc. of 18th International Conference on Pattern Recognition*, volume 1, pages 1022–1025, August 2006. 4

[13] B. Zitova and J. Flusser. Image registration methods: a survey. *Image and Vision Computing*, 21(11):977–1000, October 2003. 2

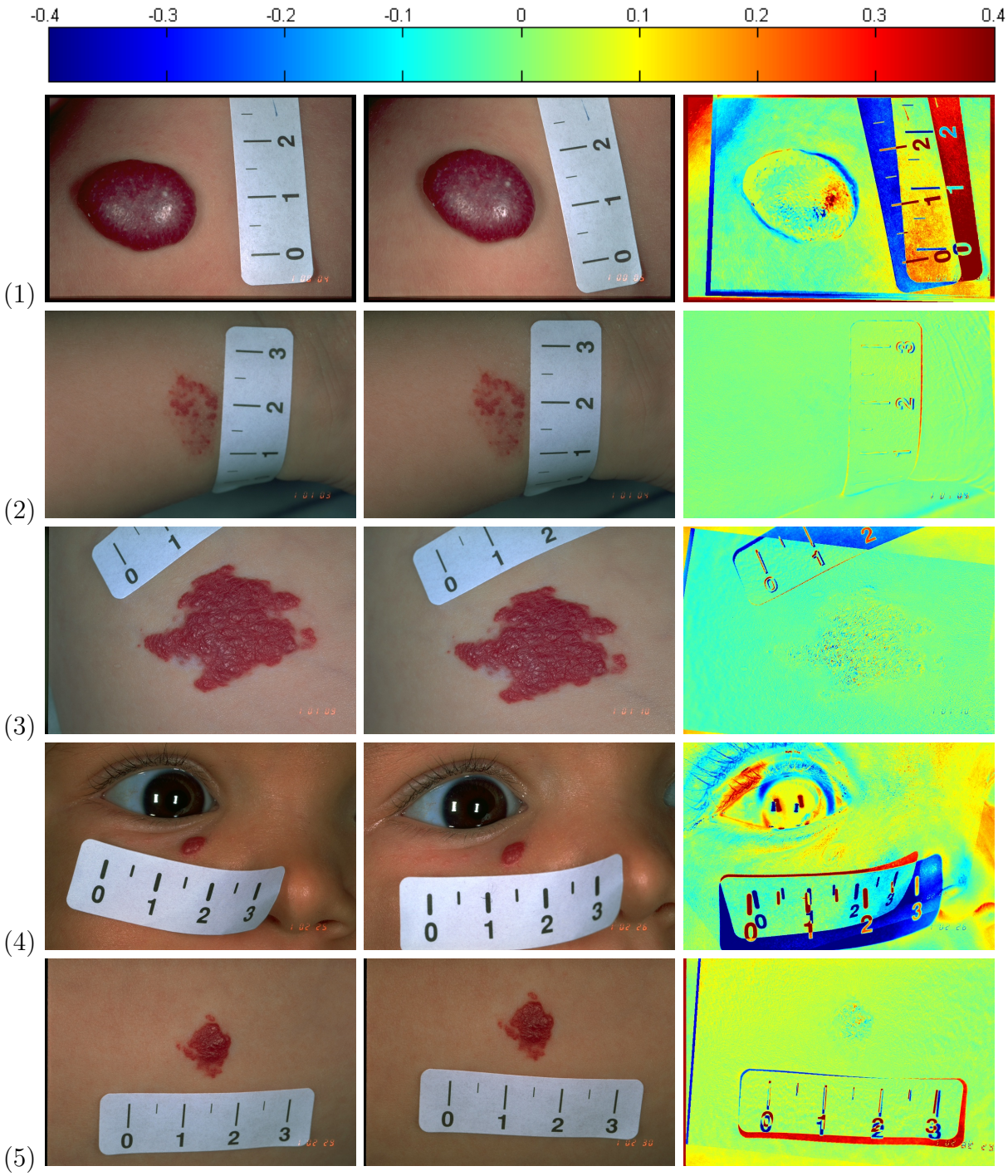

Figure 8: Difference images (1)-(5) of totally 20 registered image pairs showing the same hemangioma at the same time. The colorbar is shown at the top.

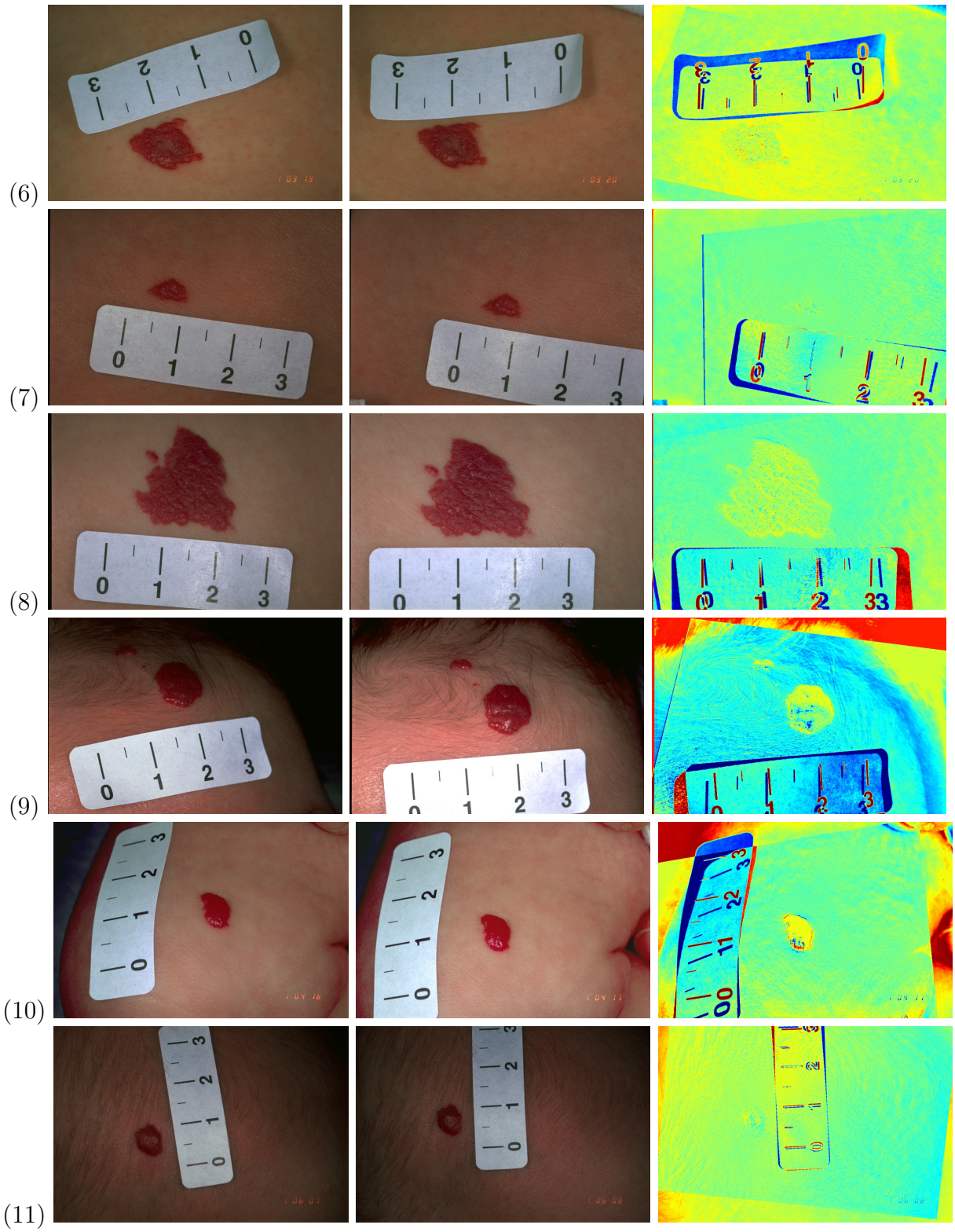

Figure 9: Difference images (5)-(11) of totally 20 registered image pairs showing the same hemangioma at the same time.

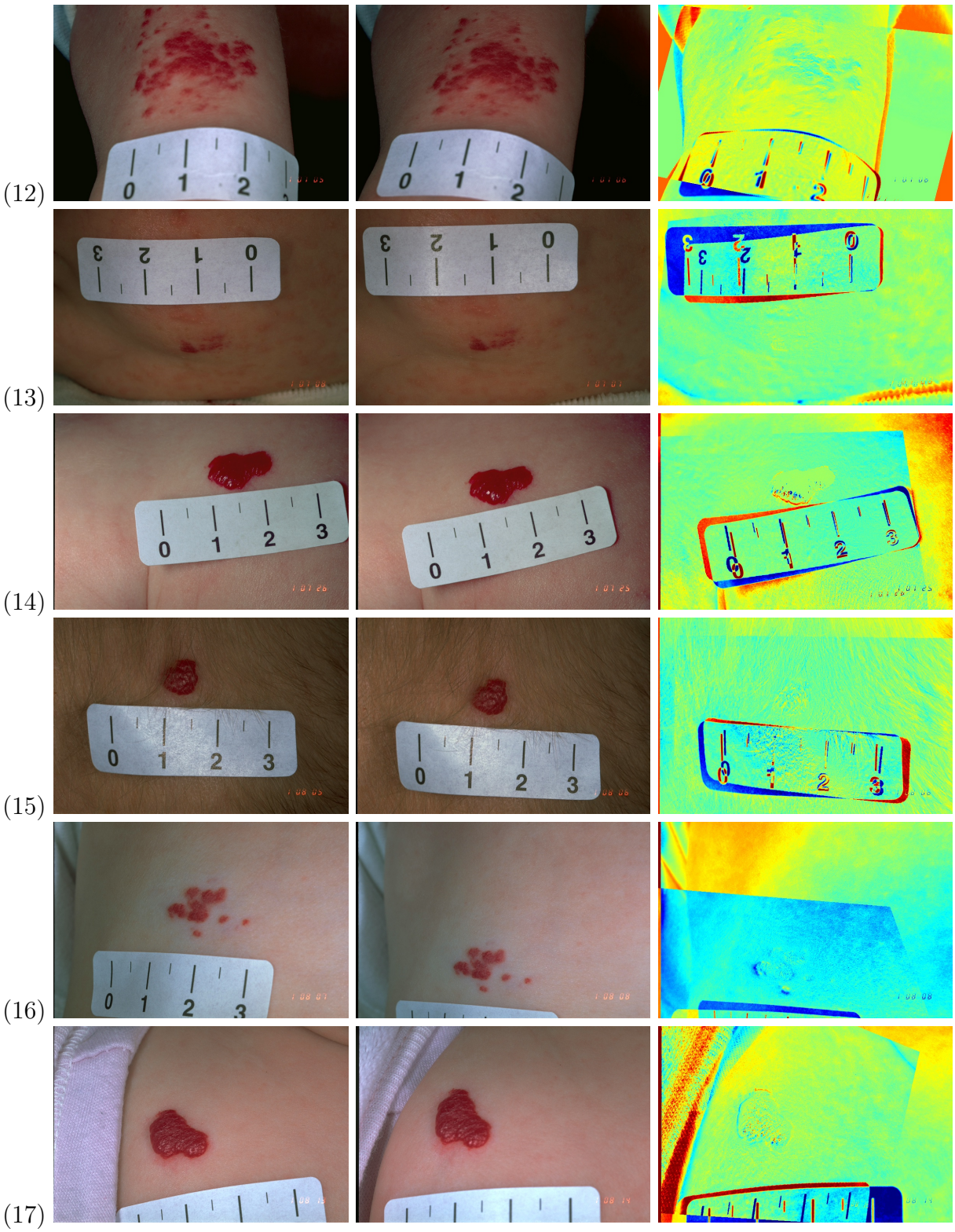

Figure 10: Difference images (12)-(17) of totally 20 registered image pairs showing the same hemangioma at the same time.

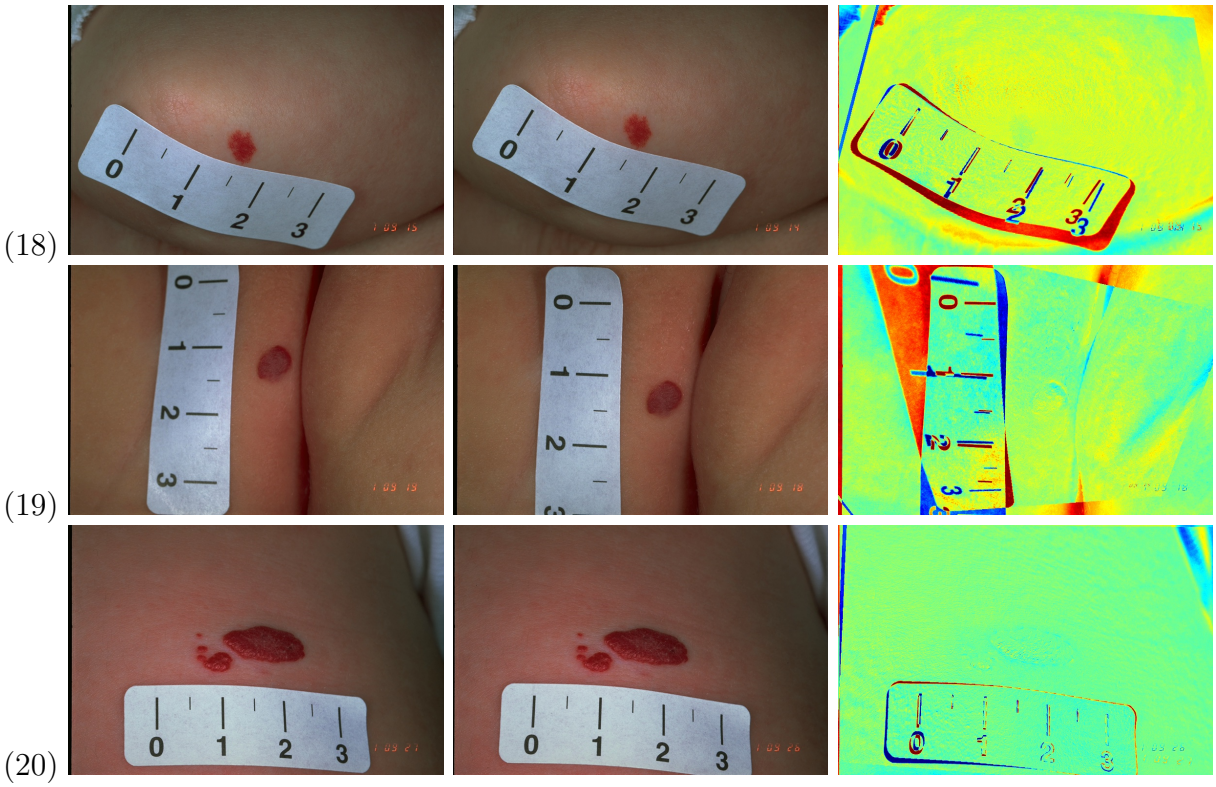

Figure 11: Difference images (18)-(20) of totally 20 registered image pairs showing the same hemangioma at the same time.

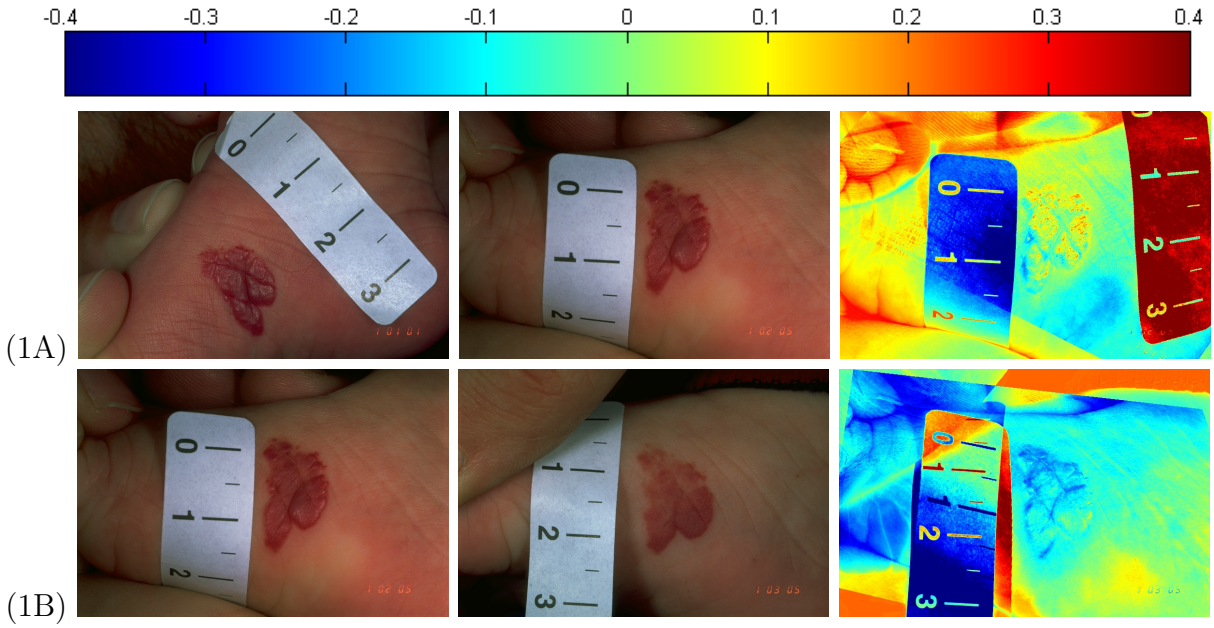

Figure 12: Difference images (1A)-(1B) of totally 13 registered image pairs showing the same hemangioma at different times. The colorbar is shown at the top.

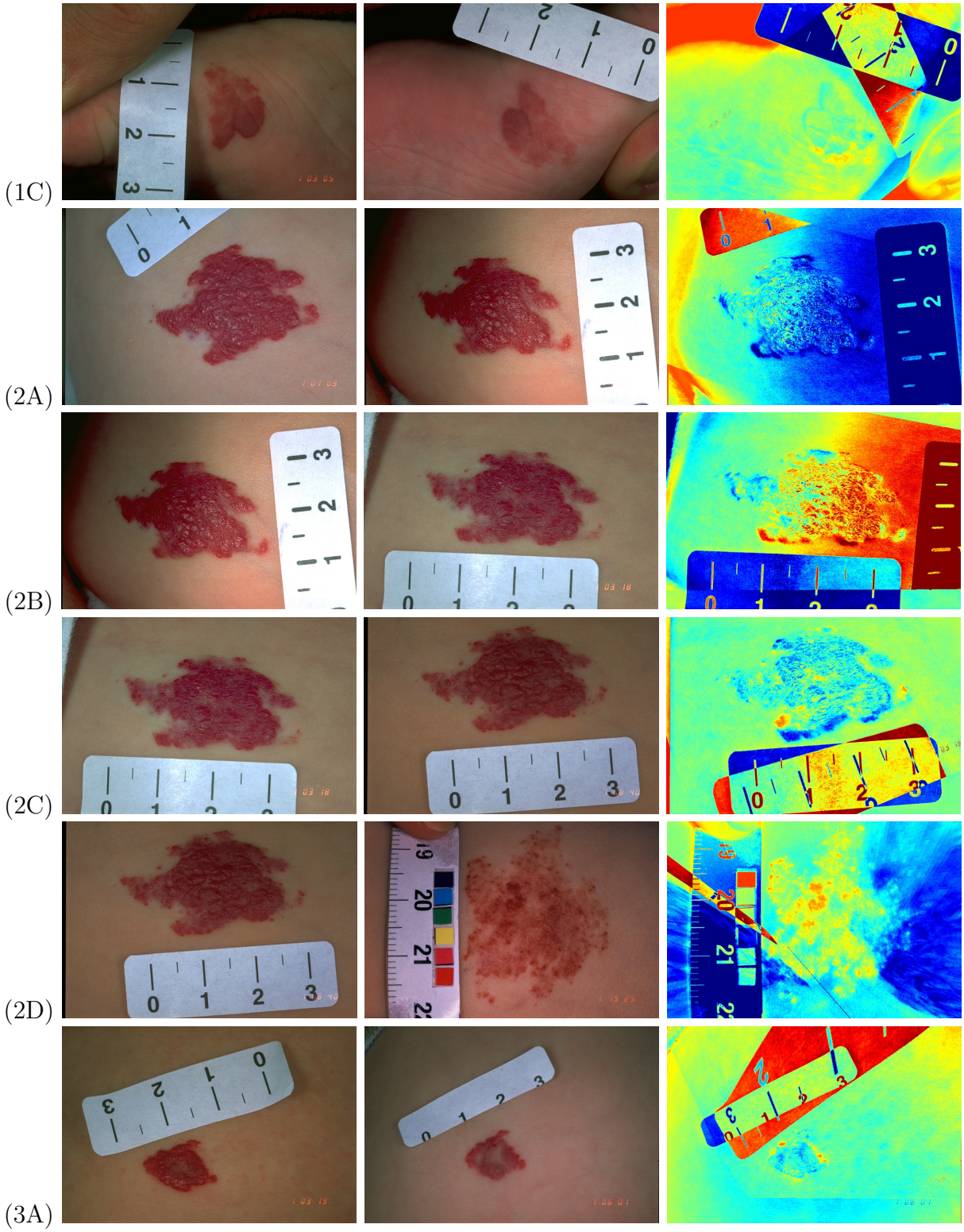

Figure 13: Difference images (1C)-(3A) of totally 13 registered image pairs showing the same hemangioma at different times.

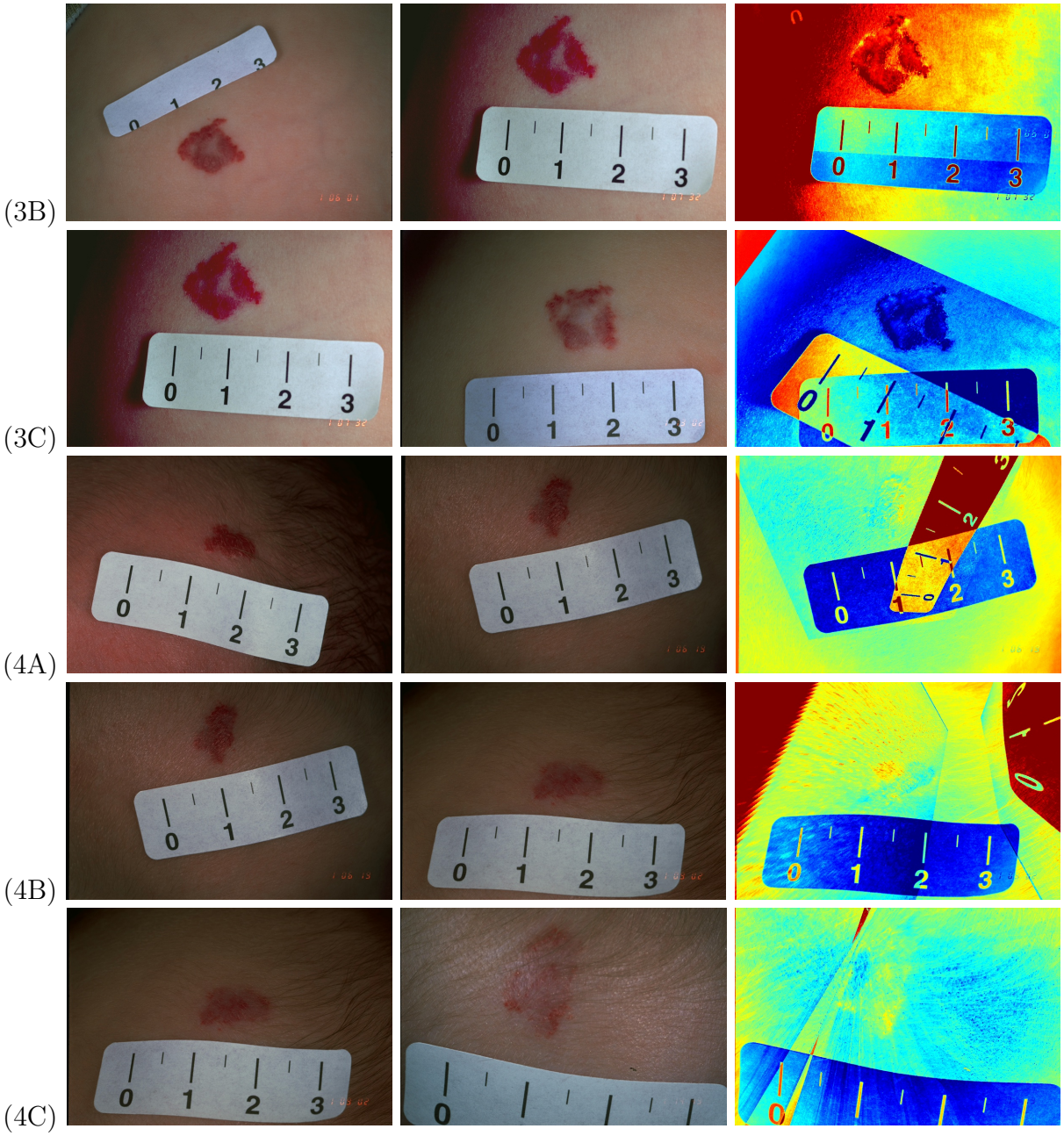

Figure 14: Difference images (3B)-(4C) of totally 13 registered image pairs showing the same hemangioma at different times.